

Production of high-spin ω_J/ρ_J ($J = 2, 3, 4, 5$) mesons in $\pi^- p$ reactions

Ting-Yan Li^{1,2,3,4,*}, Zi-Yue Bai^{1,2,3,4,†} and Xiang Liu^{1,2,3,4,‡}

¹*School of Physical Science and Technology, Lanzhou University, Lanzhou 730000, China*

²*Lanzhou Center for Theoretical Physics, Key Laboratory of Theoretical Physics of Gansu Province, Key Laboratory of Quantum Theory and Applications of MoE,*

Gansu Provincial Research Center for Basic Disciplines of Quantum Physics, Lanzhou University, Lanzhou 730000, China

³*MoE Frontiers Science Center for Rare Isotopes, Lanzhou University, Lanzhou 730000, China*

⁴*Research Center for Hadron and CSR Physics, Lanzhou University and Institute of Modern Physics of CAS, Lanzhou 730000, China*

(Dated: March 12, 2026)

In this work, we perform a comprehensive investigation of the production of high-spin ω_J and ρ_J mesons ($J = 2, 3, 4, 5$) in $\pi^- p$ reactions using an effective Lagrangian approach. By constructing the relevant t -channel processes and calibrating the model with a single adjustable parameter fitted to existing data, we successfully reproduce the measured total and differential cross sections for the $J = 3$ states $\omega_3(1670)$ and $\rho_3(1690)$. Within the same framework, we predict the production cross sections for their lower- and higher-spin partners: $\omega_2(1975)$, $\rho_2(1940)$, $\omega_4(2250)$, $\rho_4(2230)$, $\omega_5(2350)$, and $\rho_5(2350)$. Our results show that these states exhibit measurable cross sections with characteristically forward-peaked angular distributions, underscoring their strong potential for observation in future πp meson-beam experiments.

I. INTRODUCTION

Over the past several decades, accelerator experiments have played an increasingly important role in exploring new phenomena in particle physics. However, when examining the status of light hadrons compiled by the Particle Data Group (PDG) [1], it should be noted that the establishment of the light-hadron spectrum owes largely to meson-beam experiments (see review [2]). This historical fact underscores the continued relevance of πp and $K p$ scattering studies today, even in the era of running experiments such as BESIII, Belle II, and LHCb. Building upon this perspective, numerous theoretical studies in recent years have focused on light hadrons produced in πp and $K p$ reactions [3–9]. These investigations provide crucial information for elucidating the spectroscopy of such states, underscoring the importance of establishing and understanding these hadrons.

A particularly interesting subset of the light-hadron family is that of high-spin mesons, such as the ρ_J and ω_J states with $J = 2, 3, 4, 5$. Their systematics can be summarized, as shown in Fig. 1. However, precisely because of their high spin, detailed theoretical studies of these states remain relatively scarce [10–15]. Their production dynamics are thus poorly understood, making them a pertinent target for investigation.

Meson-beam experiments are uniquely suited for this task. They offer a powerful tool for discovering and studying light hadrons, as evidenced by the numerous states observed in reactions like $\pi^- p$ scattering [2]. Operating across a broad range of center-of-mass energies (from a few hundred MeV to several GeV), they probe hadrons with varying spins. The characteristically forward-peaked angular distributions in these processes further illuminate the underlying production mecha-

nisms. These features make meson-beam facilities ideal for searching not only for the high-spin ω and ρ states but also for other missing hadrons, keeping them indispensable in the ongoing effort to complete the hadron spectrum.

In this work, we investigate the production of high-spin ω_J and ρ_J mesons using an effective Lagrangian approach combined with Reggeization. The study proceeds in two stages. First, we constrain our model parameters using available data for the production of the better-established $J = 3$ states, $\omega_3(1670)$ and $\rho_3(1690)$, in $\pi^- p$ reactions. The sole free parameter is a universal cutoff, Λ_t , in the form factor. Second, employing the same model and the extracted value of Λ_t , we present predictions for the total and differential cross sections of their lower- and higher-spin partners: $\omega_2(1975)$, $\rho_2(1940)$, $\omega_4(2250)$, $\rho_4(2230)$, $\omega_5(2350)$, and $\rho_5(2350)$, whose production has not yet been measured. This approach provides a consistent, nearly parameter-free link between the known $J = 3$ sector and the unexplored $J = 2, 4, 5$ sectors, offering concrete guidance for future experimental searches.

The paper is organized as follows. Following this Introduction, Section II focuses on the production of $\omega_3(1670)$ and $\rho_3(1690)$ in πp scattering, where the model is shown to describe the available experimental data well. Based on these results, Section III presents predictions for the production characteristics of the ω and ρ states with $J = 2, 4, 5$. Finally, Section IV summarizes the work and its implications.

II. PRODUCTION OF $\omega_3(1670)$ AND $\rho_3(1690)$ IN πp REACTIONS

In this section, we present a detailed study of the πp scattering processes that produce the $J = 3$ states $\omega_3(1670)$ and $\rho_3(1690)$.

We begin by briefly summarizing the resonance parameters of the $\omega_3(1670)$ and $\rho_3(1690)$ in Table I. According to the PDG [1], the $\omega_3(1670)$ resonance was first observed in the $\pi^+ n \rightarrow p + 3\pi$ process reported in Ref. [16]. It is well established as a 1^3D_3 state and its dominant decay channels include

*Electronic address: lity2023@lzu.edu.cn

†Electronic address: baiziyue@lzu.edu.cn

‡Electronic address: xiangliu@lzu.edu.cn

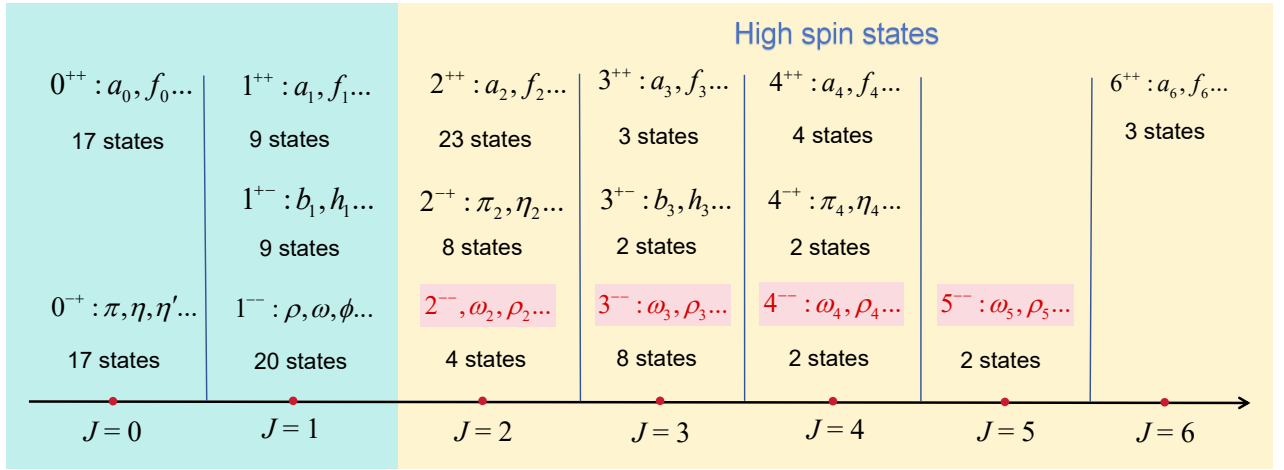


FIG. 1: A concise summary of light mesons [1].

$\rho\pi$, $\rho\pi\pi$, and $b_1(1235)\pi$, as listed in the PDG.

The $\rho_3(1690)$ state, as the isovector partner of the $\omega_3(1670)$, has been extensively studied in various production channels, such as $\pi^- p \rightarrow p + 3\pi$, $\pi^- p \rightarrow K^+ K^- n$, $\pi^- p \rightarrow p + 4\pi$, and $\pi^- p \rightarrow \eta\pi^- \pi^+ n$, among others [1]. Its decay modes are diverse, including 4π , $\pi\pi$, $\omega\pi$, $a_2(1320)\pi$, $\rho\rho$, $\phi\pi$, $\eta\pi$, and several other final states.

TABLE I: The experimental information of the $\omega_3(1670)$ and $\rho_3(1690)$ states. Here, the masses and widths are average values taken from the PDG [1].

$I(J^{PC})$	States	Mass (MeV)	Width (MeV)
$0(3^{--})$	$\omega_3(1670)$	1677 ± 4	168 ± 10
$1(3^{--})$	$\rho_3(1690)$	1686 ± 4	186 ± 14

Following the review of the experimental status of the $\omega_3(1670)$ and $\rho_3(1690)$ mesons, the quark pair creation (QPC) model is adopted to quantitatively calculate their dominant decay modes [14, 15]. The corresponding branching ratios obtained within the QPC model are listed in Table II, which show good overall agreement with the available experimental data.

For the $\omega_3(1670)$, the dominant decay mode is $\pi\rho$ with a branching ratio of 0.66, followed by significant contributions from πb_1 and $\eta\omega$. In contrast, the $K\bar{K}$ and $K\bar{K}^*$ channels are highly suppressed, each with a branching ratio of only 0.003.

For the $\rho_3(1690)$, the largest decay channel is $\rho\rho$ with a branching ratio of 0.55. Subleading contributions come from $\pi\pi$ and $\pi\omega$, while πh_1 , πa_2 , $\eta\rho$, πa_1 , and $K\bar{K}$ exhibit smaller but non-negligible branching ratios.

While the decay properties of these mesons have been studied theoretically, a systematic analysis of their production dynamics remains to be fully explored. The $\pi^- p$ scattering process provides a suitable framework for this investigation, as both states have been historically observed in such reactions [17, 18]. The feasibility of this approach is strongly supported by their decay patterns. Specifically, the $\omega_3(1670)$

decays predominantly via $\pi\rho$ (branching ratio 0.66), while the $\rho_3(1690)$ has a significant $\pi\pi$ decay component. The prominence of these π -containing final states makes a description via t -channel meson exchange particularly natural. As shown in the tree-level Feynman diagrams in Fig. 2, the process $\pi^- p \rightarrow \omega_3(1670)n$ can proceed via ρ -meson exchange, and $\pi^- p \rightarrow \rho_3(1690)n$ via π -meson exchange.

TABLE II: The partial decay channels of the $\omega_3(1670)$ and $\rho_3(1690)$ states [14, 15].

$\omega_3(1670)$		$\rho_3(1690)$	
Channel	BR	Channel	BR
$\pi\rho$	0.66	$\rho\rho$	0.55
πb_1	0.24	$\pi\pi$	0.17
$\eta\omega$	0.04	$\pi\omega$	0.12
$K\bar{K}$	0.003	πh_1	0.06
$K\bar{K}^*$	0.003	πa_2	0.04
		$\eta\rho$	0.02
		πa_1	0.02
		$K\bar{K}$	0.01

In studying the reactions $\pi^- p \rightarrow \omega_3(1670)n$ and $\pi^- p \rightarrow \rho_3(1690)n$, we consider only the dominant t -channel contributions, as illustrated in Fig. 2. The s -channel contributions are highly suppressed because the intermediate nucleon pole mass lies far below the production threshold of the final-state ω_3/ρ_3 and n . The u -channel contributions are also negligible, as the baryon-antibaryon decay modes of these states are kinematically disfavored or experimentally insignificant. We therefore employ an effective Lagrangian approach to calculate the corresponding t -channel amplitudes.

The reaction $\pi^- p \rightarrow \omega_3(1670)n$ [Fig. 2(a)]. The reaction $\pi^- p \rightarrow \omega_3(1670)n$ proceeds dominantly via t -channel ρ -

meson exchange. This mechanism is strongly supported by the decay properties of the $\omega_3(1670)$, in particular its dominant decay into $\pi\rho$ with a branching fraction of about 66%. Although the decay $\omega_3 \rightarrow \pi b_1$ is also allowed, the corresponding t -channel exchange of a b_1 meson gives a negligible contribution to the total cross section according our calculations. We consider the $W_3 V_1 P$ vertex Lagrangian [19],

$$\mathcal{L}_{W_3 V_1 P} = g_{W_3 V_1 P} \varepsilon^{\mu\nu\rho\sigma} \text{tr} \left[W_{3,\mu\alpha\beta} \left\{ (\partial_\nu V_{1,\rho}) , (\partial^\alpha \partial^\beta \partial_\sigma P) \right\}_+ \right], \quad (1)$$

where the fields W_3 , V_1 , and P correspond to the spin-3 meson with $J^{PC} = 3^-$, vector meson and pseudoscalar meson, respectively. The nonets of them read as

$$P = \frac{1}{\sqrt{2}} \begin{pmatrix} \frac{\eta+\pi^0}{\sqrt{2}} & \pi^+ & K^+ \\ \pi^- & \frac{\eta-\pi^0}{\sqrt{2}} & K^0 \\ K^- & \bar{K}^0 & \eta \end{pmatrix},$$

$$V_1^\mu = \frac{1}{\sqrt{2}} \begin{pmatrix} \frac{\omega_1^\mu + \rho_1^{0\mu}}{\sqrt{2}} & \rho_1^{+\mu} & K_1^{*+\mu} \\ \rho_1^{-\mu} & \frac{\omega_1^\mu - \rho_1^{0\mu}}{\sqrt{2}} & K_1^{*0\mu} \\ K_1^{*- \mu} & \bar{K}_1^{*0\mu} & \omega_1^\mu \end{pmatrix},$$

$$W_3^{\mu\nu\rho} = \frac{1}{\sqrt{2}} \begin{pmatrix} \frac{\omega_3^{\mu\nu\rho} + \rho_3^{0\mu\nu\rho}}{\sqrt{2}} & \rho_3^{+\mu\nu\rho} & K_3^{*+\mu\nu\rho} \\ \rho_3^{-\mu\nu\rho} & \frac{\omega_3^{\mu\nu\rho} - \rho_3^{0\mu\nu\rho}}{\sqrt{2}} & K_3^{*0\mu\nu\rho} \\ K_3^{-\mu\nu\rho} & \bar{K}_3^{*0\mu\nu\rho} & \omega_3^{\mu\nu\rho} \end{pmatrix}.$$

The specific Lagrangian we need is presented in detail as follows:

$$\mathcal{L}_{\omega_3 \rho \pi} = \frac{1}{2} g_{\omega_3 \rho \pi} \varepsilon^{\mu\nu\rho\sigma} \omega_{3,\mu\alpha\beta} (\partial_\nu \rho_\rho^+) (\partial^\alpha \partial^\beta \partial_\sigma \pi^-), \quad (2)$$

fitting the partial width $\Gamma(\omega_3(1670) \rightarrow \rho\pi) = 168$ MeV [15] yields the coupling constant $g_{\omega_3 \rho \pi} = 38.94$ GeV⁻³. The ρNN vertex is given by [20]

$$\mathcal{L}_{\rho NN} = g_{\rho NN} \bar{N} \gamma_\mu N \rho^\mu + \frac{f_{\rho NN}}{4m_p} \bar{N} \sigma_{\mu\nu} N (\partial^\mu \rho^\nu - \partial^\nu \rho^\mu), \quad (3)$$

where the values of $g_{\rho NN}$ and $f_{\rho NN}$ are listed in Table V.

The reaction $\pi^- p \rightarrow \rho_3(1690)n$ [Fig. 2(b)]. $\pi^- p \rightarrow \rho_3(1690)n$ is dominated by t -channel π -meson exchange. This choice is consistent with the decay pattern shown in Table II, where the $\pi\pi$ mode constitutes the dominant π -containing decay channel. Contributions from exchanging isoscalar mesons (e.g., ω and h_1), which correspond to different isospin processes, are neglected in the present analysis based on the available data. We consider the $W_3 PP$ vertex Lagrangian [19]:

$$\mathcal{L}_{W_3 PP} = g_{W_3 PP} \text{tr} \left[W_3^{\mu\nu\rho} \left[P, (\partial_\mu \partial_\nu \partial_\rho P) \right]_- \right], \quad (4)$$

where the fields W_3 and P correspond to the spin-3 meson with $J^{PC} = 3^-$ and two pseudoscalar mesons. The detail $\rho_3 \pi \pi$ vertex is expanded as

$$\mathcal{L}_{\rho_3 \pi \pi} = \frac{1}{2} g_{\rho_3 \pi \pi} \rho_3^{0\mu\nu\rho} \left[\pi^+ \partial_\mu \partial_\nu \partial_\rho \pi^- - \pi^- (\partial_\mu \partial_\nu \partial_\rho \pi^+) \right]. \quad (5)$$

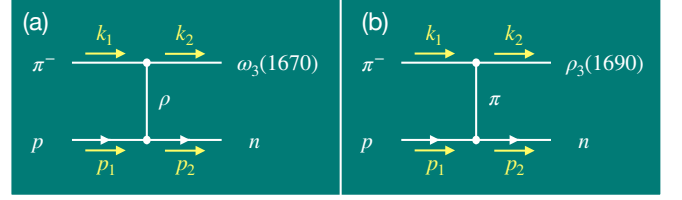


FIG. 2: Feynman diagrams for the $\pi^- p \rightarrow \omega_3(1670)n$ (a) and $\pi^- p \rightarrow \rho_3(1690)n$ (b) reactions.

Using the partial width $\Gamma(\rho_3(1690) \rightarrow \pi\pi) = 32$ MeV [14], we obtain $g_{\rho_3 \pi \pi} = 12.02$ GeV⁻². The πNN vertex is taken as [20]

$$\mathcal{L}_{NN\pi} = \frac{f_{\pi NN}}{m_\pi} \bar{\psi}_N \gamma_\mu \gamma_5 \psi_N \partial^\mu \pi, \quad (6)$$

with $f_{\pi NN} = 0.95$.

With the above Lagrangians, the amplitudes for the production of $\omega_3(1670)$ and $\rho_3(1690)$ via t -channel ρ and π exchanges in $\pi^- p$ scattering can be written as:

$$i\mathcal{M}_{\omega_3} = \frac{1}{2} g_{\omega_3 \rho \pi} \varepsilon^{\mu\nu\rho\sigma} q_\nu k_1^\alpha k_1^\beta k_{1\sigma} \varepsilon_{\mu\alpha\beta}^*(k_2) \frac{-i(g_\rho^\xi + q^\xi q_\rho / m_\rho^2)}{t - m_\rho^2} \times \bar{u}(p_2) \left(g_{\rho NN} \gamma_\xi + \frac{f_{\rho NN}}{2m_p} \gamma_\xi \not{q} \right) u(p_1) F_t(q), \quad (7)$$

$$i\mathcal{M}_{\rho_3} = -\frac{1}{2} g_{\rho_3 \pi \pi} \frac{f_{\pi NN}}{m_\pi} \bar{u}(p_2) \gamma_\sigma \gamma_5 u(p_1) q^\sigma \varepsilon_{\mu\nu\rho}^*(k_2) \times (k_{1\mu} k_{1\nu} k_{1\rho} + q_\mu q_\nu q_\rho) \frac{i}{t - m_\pi^2} F_t(q), \quad (8)$$

where $\varepsilon(k_2)$ with different index denotes the polarization vector for the $\omega_3(1670)$ and $\rho_3(1690)$. $\bar{u}(p_2)$ and $u(p_1)$ is the Dirac spinors of the nucleons. As detailed in Appendix IV, we present the complete summation formalism for the polarization tensors of the high-spin mesons with $J = 3, 4, 5$. The t is defined as the squared four-momentum transfer, $t = q^2 = (k_1 - k_2)^2$. For the t -channel meson exchange, the form factor is adopted as

$$F_t(q) = \left(\frac{\Lambda_t^2 - m^2}{\Lambda_t^2 - q^2} \right)^2, \quad (9)$$

where m represent the mass of the exchanged particle. In this study, we take into account exclusively the t -channel contribution, so that the cutoff Λ_t remains the sole adjustable parameter. By fitting the available experimental cross section data at different energies for the reaction $\pi^- p \rightarrow \omega_3(1670)n$ [16, 17, 21–23], we obtain $\Lambda_t = 3.5 \pm 0.5$ GeV, with $\chi^2/\text{d.o.f.} \leq 1.3$. Employing the same cutoff value $\Lambda_t = 3.5 \pm 0.5$ GeV for the $\pi^- p \rightarrow \rho_3(1690)n$ reaction, we find that the theoretical predictions are in good agreement with the measurements reported in Refs. [18, 24–26]. The results presented in Figs. 3 and 5, show the total cross section for the $\pi^- p \rightarrow \omega_3(1670)n$ and

$\pi^- p \rightarrow \rho_3(1690)n$ reactions calculated using $\Lambda_t = 3.5 \pm 0.5$ GeV. For the remaining processes, namely $\pi^- p \rightarrow \omega_4(2250)n$, $\pi^- p \rightarrow \omega_5(2250)n$, $\pi^- p \rightarrow \rho_4(2230)n$, $\pi^- p \rightarrow \rho_5(2350)p$, we adopt the identical cutoff $\Lambda_t = 3.5 \pm 0.5$ GeV throughout, to maintain consistency across the analyses.

The Regge trajectory model has been successfully applied to describe hadron production in the high-energy region [27, 28]. The motivation for replacing the usual Feynman propagator with a Regge propagator is to effectively account for the exchange of high-spin and high-mass states in the t channel, whose contributions cannot be neglected at higher energies. When employing conventional Feynman propagators, the resulting cross sections show a monotonically increasing dependence on the center-of-mass energy, which is inconsistent with the corresponding experimental measurements shown in Figs. 3 and 5. To address this problem, in the present framework, Reggeization is implemented by replacing the t -channel Feynman propagators in the Feynman amplitudes Eqs. (7) and (8) with the corresponding Regge propagators [29]:

$$\frac{1}{t - m_\rho^2} \rightarrow \left(\frac{s}{s_{\text{scale}}} \right)^{\alpha_\rho(t)-1} \frac{\pi \alpha'_\rho}{\Gamma[\alpha_\rho(t)] \sin[\pi \alpha_\rho(t)]}, \quad (10)$$

$$\frac{1}{t - m_\pi^2} \rightarrow \left(\frac{s}{s_{\text{scale}}} \right)^{\alpha_\pi(t)} \frac{\pi \alpha'_\pi}{\Gamma[\alpha_\pi(t) + 1] \sin[\pi \alpha_\pi(t)]}, \quad (11)$$

where the scale parameter s_{scale} is fixed at 1 GeV. The functions $\alpha_\rho(t)$ and $\alpha_\pi(t)$ denote the (J, M^2) Regge trajectories [29, 30]:

$$\alpha_\rho(t) = 1 + \alpha'_\rho(t - m_\rho^2), \quad (12)$$

$$\alpha_\pi(t) = \alpha'_\pi(t - m_\pi^2). \quad (13)$$

where $\alpha'_\rho = 0.8 \text{ GeV}^{-2}$ and $\alpha'_\pi = 0.7 \text{ GeV}^{-2}$ are the slopes of the corresponding Regge trajectories, which can be generally constrained by the experimentally established states lying on the same trajectories [29, 30].

Based on the preceding theoretical framework, the cross section for the reaction $\pi^- p \rightarrow \omega_3(1670)n$ and $\pi^- p \rightarrow \rho_3(1690)n$ can be calculated. The differential cross section in the center-of-mass (c.m.) frame is given by

$$\frac{d\sigma}{d \cos \theta} = \frac{1}{32\pi s} \frac{|\vec{k}_2^{\text{c.m.}}|}{|\vec{k}_1^{\text{c.m.}}|} \left(\frac{1}{2} \sum_\lambda |\mathcal{M}|^2 \right), \quad (14)$$

where $s = (k_1 + p_1)^2$ is defined, and θ is the angle between the outgoing meson and the incident π^- beam direction in the c.m. frame. The three-momenta $\vec{k}_1^{\text{c.m.}}$ and $\vec{k}_2^{\text{c.m.}}$ correspond to the initial π^- beam and the final meson, respectively. The factor of $1/2$ accounts for the average over the initial nucleon spin states.

Numerical results. The total cross section for the reaction $\pi^- p \rightarrow \omega_3(1670)n$ is presented in Fig. 3. The experimental data (black points with error bars) are compiled from

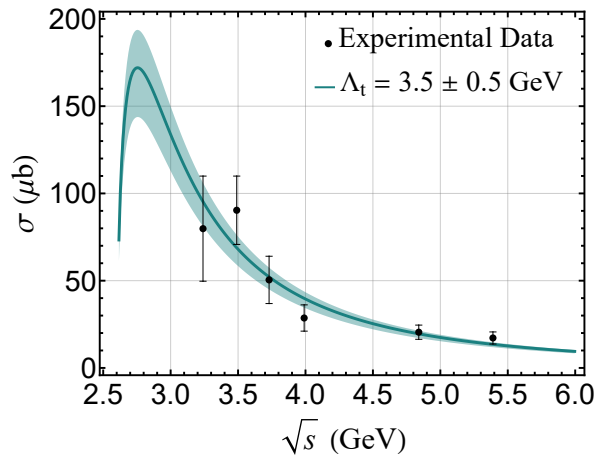


FIG. 3: The total cross section for the reaction $\pi^- p \rightarrow \omega_3(1670)n$. The black points with error bars correspond to the experimental data from Refs. [16, 17, 21–23].

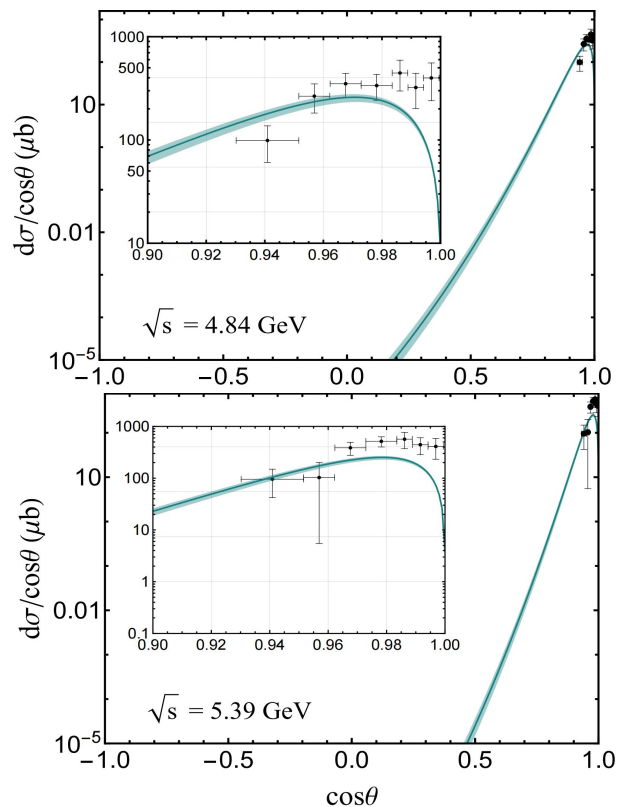


FIG. 4: The differential cross section $d\sigma/d \cos \theta$ of the $\omega_3(1670)$ production at different c.m. energy E_{cm} . The black points with error bars correspond to the experimental data from Ref. [17].

Refs. [16, 17, 21–23]. The theoretical calculation, with a cutoff parameter $\Lambda_t = 3.5$ GeV, is shown as the green solid curve. The associated uncertainty, estimated by varying Λ_t by ± 0.5 GeV, is represented by the green band. The theoretical curve closely follows the overall trend of the data across the measured energy range, demonstrating good agreement.

Among the data points in Fig. 3, differential cross-section measurements are available only for the last two (highest) center-of-mass energies. To examine the angular distributions, the differential cross sections $d\sigma/d\cos\theta$ at $E_{\text{cm}} = 4.84$ GeV and 5.39 GeV are presented in Fig. 4, together with the corresponding experimental data from Ref. [17]. The data are concentrated at forward angles ($\cos\theta$ close to 1). For clearer comparison, subplots focusing on the region $0.90 < \cos\theta < 1.00$ are included in Fig. 4.

At $E_{\text{cm}} = 4.84$ GeV, the theoretical prediction (green solid curve) agrees excellently with the data over the full angular range, accurately reproducing a characteristic dip near $\cos\theta \approx 0.98$. At $E_{\text{cm}} = 5.39$ GeV, slight deviations appear at very forward angles (around $\cos\theta \approx 0.97$). Nevertheless, the overall shape of the angular distribution, particularly its pronounced forward peaking, is well reproduced by the calculation. Although not all data points are encompassed at this higher energy, the theoretical curve captures the essential features of the measured distribution.

In summary, using the cutoff $\Lambda_t = 3.5 \pm 0.5$ GeV, our calculations provide a satisfactory description of both the total and differential cross sections for $\pi^- p \rightarrow \omega_3(1670)n$. This agreement supports the adequacy of the chosen parameter for modeling $\omega_3(1670)$ production in this reaction.

The production of the $\rho_3(1690)$ state in $\pi^- p$ scattering is analyzed within the same theoretical model used for the $\omega_3(1670)$. For consistency, we adopt the same cutoff parameter $\Lambda_t = 3.5$ GeV and its associated uncertainty ± 0.5 GeV to estimate the theoretical band, as shown in Figs. 5 and 6.

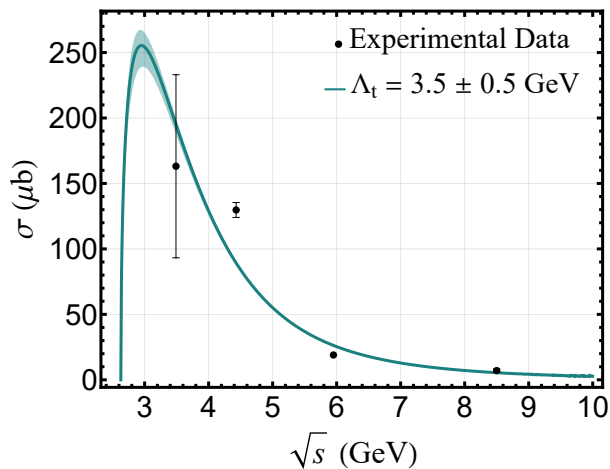


FIG. 5: The total cross section for the reaction $\pi^- p \rightarrow \rho_3(1690)n$. The black points with error bars correspond to the experimental data from Refs. [18, 24–26].

Figure 5 presents the total cross section for $\pi^- p \rightarrow \rho_3(1690)n$. The experimental data from Refs. [18, 24–26] (black points with error bars) are well described within the theoretical uncertainty band across the displayed energy range. The theoretical curve reproduces the trend of the data, the cross section rises to a maximum around $\sqrt{s} \approx 2.9$ GeV and then gradually decreases as the energy increases.

A more detailed angular analysis is provided in Fig. 6,

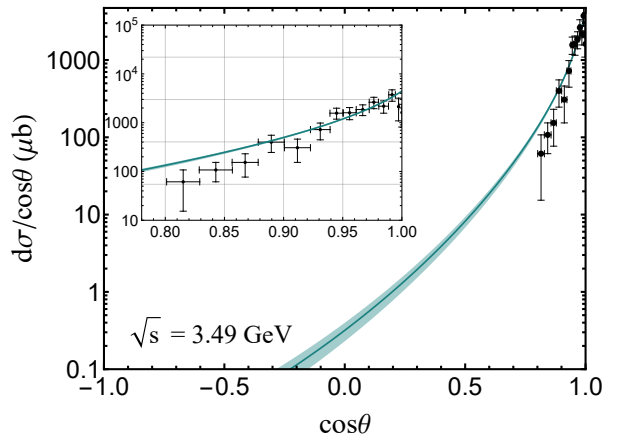


FIG. 6: The differential cross section $d\sigma/d\cos\theta$ of the $\rho_3(1690)$ production at c.m. energy $E_{\text{cm}} = 3.49$ GeV. The black points with error bars correspond to the experimental data from Ref. [18].

which shows the differential cross section $d\sigma/d\cos\theta$ at $\sqrt{s} = 3.49$ GeV. The theoretical prediction (solid green curve) and its associated uncertainty band (corresponding to $\Lambda_t = 3.5 \pm 0.5$ GeV) are compared with the experimental data from Ref. [18]. The predicted angular distribution exhibits a pronounced forward peak ($\cos\theta \rightarrow 1$). Excellent agreement with the data is achieved in this forward region, as clearly shown in the magnified inset.

With the parameter choice of $\Lambda_t = 3.5 \pm 0.5$ GeV, the model yields a consistent and satisfactory description of both the total and differential cross sections for $\omega_3(1670)$ and $\rho_3(1690)$ production. This agreement supports the validity of the adopted theoretical framework and indicates its reliability in capturing the production dynamics of these two $J = 3$ mesons, which share the same J^{PC} quantum numbers but differ in isospin.

We note that the structures in the effective Lagrangians for high-spin fields are not uniquely determined. In this work, we adopt the minimal derivative rule: for each vertex, we retain the lowest number of derivatives consistent with Lorentz invariance and parity conservation. The coupling constants are fixed by the corresponding partial decay widths. Hence, any alternative Lagrangian form that reproduces the same width would yield a proportionally adjusted coupling, leaving the overall scale of the cross section largely unchanged. The validity of our minimal choice at low energies is explicitly verified by the successful fit to the $J = 3$ total and differential cross section data.

At high energies, the Reggeization of t -channel propagators further reduces the sensitivity to vertex details. The Regge amplitude is dominated by the universal Regge trajectory $\alpha(t)$, which governs the energy dependence, while the vertex structure contributes only to the residue. Consequently, the predicted production features for the $J = 4, 5$ states are robust against moderate variations in the Lagrangian construction, as shown in the following section.

III. PRODUCTION OF HIGHER-SPIN ω_J/ρ_J ($J = 4, 5$) MESONS IN $\pi^- p$ REACTIONS

We now extend the same theoretical framework to predict the production cross sections of the lower-spin and higher-spin ω_J and ρ_J mesons ($J = 2, 4, 5$) in $\pi^- p$ reactions. This section is organized as follows. After a brief review of the experimental status of these states, we outline the theoretical formalism, including the effective Lagrangians and production amplitudes. Finally, we present the predicted total and differential cross sections.

The resonance parameters for the ω_J and ρ_J mesons with $J = 2, 3, 4$ and 5 are summarized in Table III. These states are the natural lower-spin and higher-spin partners of the $J = 3$ $\omega_3(1670)$ and $\rho_3(1690)$. According to the PDG [1], the $\omega_2(1975)$, $\rho_2(1940)$, $\omega_4(2250)$, $\rho_4(2230)$, and $\omega_5(2250)$ are categorized as ‘‘further states,’’ requiring more confirmation, whereas the $\rho_5(2350)$ is more firmly established.

Experimentally, these states have been observed in specific production channels. The $\omega_2(1975)$ and $\omega_4(2250)$ are seen in $p\bar{p}$ annihilation, e.g., $p\bar{p} \rightarrow \omega\eta$ and $p\bar{p} \rightarrow \omega\pi^0\pi^0$ [31]. Similarly, the $\rho_2(1940)$ and $\rho_4(2230)$ are found in $p\bar{p} \rightarrow \omega\pi^0$, $p\bar{p} \rightarrow \omega\eta\pi^0$, and $p\bar{p} \rightarrow \pi^+\pi^-$ [32]. The $\omega_5(2250)$ was only seen in $p\bar{p} \rightarrow \omega\eta$ and $p\bar{p} \rightarrow \omega\pi^0\pi^0$ [31, 33], while the $\rho_5(2350)$ has been identified in several reactions, including $\pi^- p \rightarrow \omega\pi^0 n$, $p\bar{p} \rightarrow \pi\pi$, and $p\bar{p} \rightarrow K^+K^-$ [26, 34, 35].

Several features can be inferred from the PDG values listed in Table III. For $J = 2$, the isoscalar $\omega_2(1975)$ has a mass of 1975 ± 20 MeV and a width of 175 ± 25 MeV, while the isovector $\rho_2(1940)$ has a mass of 1940 ± 40 MeV and a width of 155 ± 40 MeV. The mass splitting between ω_2 and ρ_2 is approximately 35 MeV, which is relatively small, and their widths are comparable. Moving to $J = 4$, the isoscalar $\omega_4(2250)$ and the isovector $\rho_4(2230)$ have comparable masses around 2.24 GeV, with the ρ_4 being slightly lighter. Their total widths are of order 150–210 MeV. For $J = 5$, the $\omega_5(2250)$ and $\rho_5(2350)$ are heavier and exhibit significantly larger widths. Notably, the mass splitting between ω_J and ρ_J partners is small for $J = 4$, but becomes more pronounced for $J = 5$, reaching about 80 MeV, with the ρ_5 being the heavier state.

TABLE III: The experimental information of the ω_J/ρ_J ($J = 2, 4, 5$) mesons. Here, the masses and widths are average values taken from the PDG [1].

$I(J^{PC})$	States	Mass (MeV)	Width (MeV)
0 (2^-)	$\omega_2(1975)$	1975 ± 20	175 ± 25
1 (2^-)	$\rho_2(1940)$	1940 ± 40	155 ± 40
0 (4^-)	$\omega_4(2250)$	2250 ± 30	150 ± 50
1 (4^-)	$\rho_4(2230)$	2230 ± 25	210 ± 30
0 (5^-)	$\omega_5(2250)$	2250 ± 70	320 ± 95
1 (5^-)	$\rho_5(2350)$	2330 ± 35	400 ± 100

We now examine the theoretical decay properties of the ω_J and ρ_J ($J = 2, 4, 5$) mesons. Their predicted partial de-

cay channels and corresponding branching ratios, calculated within the QPC model [15], are compiled in Table IV.

For the $\omega_2(1975)$, the dominant decay channel is $\pi\rho(1450)$ with a branching ratio of 0.48, indicating a strong preference for decay into a pseudoscalar meson and an excited vector meson. The channel $\pi\rho$ also contributes significantly with a branching ratio of 0.24. Other notable channels include πb_1 (0.11) and $\pi\rho_3(1690)$ (0.07). For the $\rho_2(1940)$, the largest decay channel is $\pi a_2(1320)$ with a branching ratio of 0.25, highlighting decays into a pseudoscalar and a tensor meson. The channel $\pi\omega(1420)$ has a branching ratio of 0.21, and the $\pi\omega$ contributes 0.15. Other significant channels include $\pi h_1(1170)$ and $\rho\eta$.

For the $\omega_4(2250)$, the QPC model identifies the $a_1\rho$ and $a_2\rho$ channels as dominant, indicating a preference for decays into an axial-vector or tensor meson plus a vector meson. The decay ωf_2 also contributes significantly. In contrast, the $\rho_4(2230)$ is predicted to decay predominantly into ρb_1 and $\rho\rho$, highlighting decays involving an excited axial-vector b_1 or a pair of vector mesons.

For the $J = 5$ states, the $\omega_5(2250)$ has a very large branching fraction into ρa_2 (branching ratio ≈ 0.58), followed by ωf_2 . The $\rho_5(2350)$ does not exhibit a single overwhelmingly dominant channel; its largest decay channels are ρf_2 and ωa_2 , each with a branching ratio of 0.24, alongside smaller but notable contributions from ρb_1 and $\rho\rho$. These predictions provide a specific, testable framework for the decay properties of these higher-spin states.

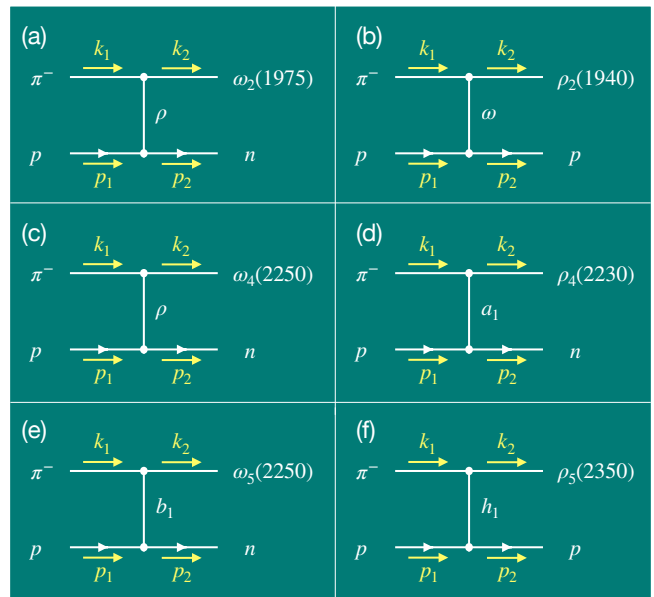


FIG. 7: Feynman diagrams for the $\pi^- p \rightarrow \omega_J/\rho_J + N$ reactions.

Production mechanism. Building on the successful description of $\omega_3(1670)$ and $\rho_3(1690)$ production in $\pi^- p$ scattering using a universal cutoff $\Lambda_t = 3.5 \pm 0.5$ GeV, the similiar framework is further employed to predict the production of the corresponding lower-spin and higher-spin partners.

The phenomenological basis for this extension lies in the

decay patterns predicted by the QPC model (Table IV). Although not always the dominant modes, decays such as $\omega_4 \rightarrow \pi\rho$ and $\rho_4 \rightarrow \pi a_1$ occur with non-negligible branching ratios. This indicates that these states can be produced in $\pi^- p$ reactions via t -channel single-meson exchange, in direct analogy to the $J = 3$ case. The choice of the exchanged meson in the t -channel is guided by the dominant π -containing decay modes predicted by the QPC model (Table IV). The corresponding tree-level Feynman diagrams for the reactions $\pi^- p \rightarrow \omega_2(1975)n$, $\pi^- p \rightarrow \rho_2(1940)p$, $\pi^- p \rightarrow \omega_4(2250)n$, $\pi^- p \rightarrow \rho_4(2230)n$, $\pi^- p \rightarrow \omega_5(2250)n$, and $\pi^- p \rightarrow \rho_5(2350)^- p$ are depicted in Fig. 7(a)-(f), respectively. Given the limited existing experimental data on their production, these parameter-free predictions offer valuable guidance for future investigations in this energy region.

All upper vertices (three-meson couplings) in Fig. 7 are constructed in this work. Their effective Lagrangians, written in terms of the tensor fields W_J for the high-spin states, are given below. The lower vertices (meson-nucleon-nucleon couplings) are taken from the established phenomenological Lagrangians [36].

$\pi^- p \rightarrow \omega_2(1975)n$ [Fig. 7(a)]. This reaction proceeds via ρ -meson exchange, motivated by the fact that $\pi\rho$ is the most prominent π -containing decay of $\omega_2(1975)$ (Table IV). The effective Lagrangian for the $W_2 V_1 P$ vertex is

$$\mathcal{L}_{W_2 V_1 P} = g_{W_2 V_1 P} \text{tr} \left[W_2^{\alpha\beta} \{V_\alpha, \partial_\beta P\}_+ \right], \quad (15)$$

where the fields W_2 , V_1 , and P correspond to the spin-2 meson with $J^{PC} = 2^{--}$, vector meson and pseudoscalar meson, respectively. The nonet of 2^{--} reads

$$W_2^{\mu\nu} = \frac{1}{\sqrt{2}} \begin{pmatrix} \frac{\omega_2^{\mu\nu} + \rho_2^{0\mu\nu}}{\sqrt{2}} & \rho_2^{+\mu\nu} & K_2^{+\mu\nu} \\ \rho_2^{-\mu\nu} & \frac{\omega_2^{\mu\nu} - \rho_2^{0\mu\nu}}{\sqrt{2}} & K_2^{0\mu\nu} \\ K_2^{-\mu\nu} & \bar{K}_2^{0\mu\nu} & \omega_2^{\mu\nu} \end{pmatrix}.$$

The specific form of the $\omega_2\rho\pi$ vertex is as follows:

$$\mathcal{L}_{\omega_2\rho\pi} = \frac{1}{2} g_{\omega_2\rho\pi} \omega_2^{\alpha\beta} \rho_\alpha^+ \partial_\beta \pi^-. \quad (16)$$

The ρNN vertex is presented in Eq. (3).

$\pi^- p \rightarrow \rho_2(1940)p$ [Fig. 7(b)]. The forms of the Lagrangian for the two vertices in this process are exactly the same as that in the previous process ($\pi^- p \rightarrow \omega_2(1975)n$), with only the exchanged particle changed from ρ to ω . Hence, we omit the Lagrangian required for this Feynman process here.

$\pi^- p \rightarrow \omega_4(2250)n$ [Fig. 7(c)]. This reaction proceeds via ρ -meson exchange, motivated by the fact that $\pi\rho$ is the most prominent π -containing decay of $\omega_4(2250)$ (Table IV). The effective Lagrangian for the $W_4 V_1 P$ vertex is

$$\mathcal{L}_{W_4 V_1 P} = g_{W_4 V_1 P} \text{tr} \left[W_4^{\mu\nu\alpha\beta} \{V_\mu, \partial_\nu \partial_\alpha \partial_\beta P\}_+ \right], \quad (17)$$

where the fields W_4 , V_1 , and P correspond to the spin-4 meson with $J^{PC} = 4^{--}$, vector meson and pseudoscalar meson,

respectively. The nonet of 4^{--} reads

$$W_4^{\mu\nu\rho\sigma} = \frac{1}{\sqrt{2}} \begin{pmatrix} \frac{\omega_4^{\mu\nu\rho\sigma} + \rho_4^{0\mu\nu\rho\sigma}}{\sqrt{2}} & \rho_4^{+\mu\nu\rho\sigma} & K_4^{+\mu\nu\rho\sigma} \\ \rho_4^{-\mu\nu\rho\sigma} & \frac{\omega_4^{\mu\nu\rho\sigma} - \rho_4^{0\mu\nu\rho\sigma}}{\sqrt{2}} & K_4^{0\mu\nu\rho\sigma} \\ K_4^{-\mu\nu\rho\sigma} & \bar{K}_4^{0\mu\nu\rho\sigma} & \omega_4^{\mu\nu\rho\sigma} \end{pmatrix}.$$

The specific form of the $\omega_4\rho\pi$ vertex is as follows:

$$\mathcal{L}_{\omega_4\rho\pi} = \frac{1}{2} g_{\omega_4\rho\pi} \omega_4^{\sigma\alpha\beta\gamma} \rho_\sigma^+ \partial_\alpha \partial_\beta \partial_\gamma \pi^-. \quad (18)$$

The ρNN vertex is presented in Eq. (3).

$\pi^- p \rightarrow \rho_4(2230)n$ [Fig. 7(d)]. The dominant π -containing decay πa_1 leads to a_1 -meson exchange. The effective Lagrangian is

$$\mathcal{L}_{W_4 A_1 P} = g_{W_4 A_1 P} \epsilon_{\mu\nu\rho\sigma} \text{tr} \left[W_4^{\mu\alpha\beta\gamma} [(\partial^\nu A_1^\rho), (\partial_\alpha \partial_\beta \partial_\gamma \partial^\sigma P)]_- \right], \quad (19)$$

where the fields W_4 , A_1 , and P correspond to the spin-4 meson with $J^{PC} = 4^{--}$, axial-vector meson and pseudoscalar meson, respectively. The matrix A_1 has the form

$$A_1^\mu = \frac{1}{\sqrt{2}} \begin{pmatrix} \frac{f_1^\mu + a_1^{0\mu}}{\sqrt{2}} & a_1^{+\mu} & K_{1,A}^{+\mu} \\ a_1^{-\mu} & \frac{f_1^\mu - a_1^{0\mu}}{\sqrt{2}} & K_{1,A}^{0\mu} \\ K_{1,A}^{-\mu} & \bar{K}_{1,A}^{0\mu} & f_1^\mu \end{pmatrix}.$$

The Lagrangian for $\rho_4 a_1 \pi$ vertex can be expressed in the following specific form:

$$\mathcal{L}_{\rho_4 a_1 \pi} = \frac{1}{2} g_{\rho_4 a_1 \pi} \epsilon_{\mu\nu\rho\sigma} \rho_4^{\mu\alpha\beta\gamma} (\partial^\nu a_1^{\rho+}) \partial_\alpha \partial_\beta \partial_\gamma \partial^\sigma \pi^-, \quad (20)$$

and the $a_1 NN$ vertex is taken from Ref. [36]:

$$\mathcal{L}_{a_1 NN} = g_{a_1 NN} [\bar{N} \gamma_\mu \gamma_5 N] a_1^\mu + \frac{i f_{a_1 NN}}{m_P} [\bar{N} \gamma_5 N] \partial_\mu a_1^\mu. \quad (21)$$

$\pi^- p \rightarrow \omega_5(2250)n$ [Fig. 7(e)]. This channel is dominated by t -channel b_1 exchange. The corresponding Lagrangian is

$$\mathcal{L}_{W_5 B_1 P} = g_{W_5 B_1 P} \text{tr} \left[W_5^{\mu\alpha\beta\gamma\delta} \{B_{1,\mu}, \partial_\alpha \partial_\beta \partial_\gamma \partial_\delta P\}_+ \right]. \quad (22)$$

where the fields W_5 , B_1 , and P correspond to the spin-5 meson with $J^{PC} = 5^{--}$, pseudovector meson and pseudoscalar meson, respectively. The matrix W_5 and B_1 have the form

$$W_5^{\mu\nu\rho\sigma\gamma} = \frac{1}{\sqrt{2}} \begin{pmatrix} \frac{\omega_{5N}^{\mu\nu\rho\sigma\gamma} + \rho_5^{0\mu\nu\rho\sigma\gamma}}{\sqrt{2}} & \rho_5^{+\mu\nu\rho\sigma\gamma} & K_5^{+\mu\nu\rho\sigma\gamma} \\ \rho_5^{-\mu\nu\rho\sigma\gamma} & \frac{\omega_{5N}^{\mu\nu\rho\sigma\gamma} - \rho_5^{0\mu\nu\rho\sigma\gamma}}{\sqrt{2}} & K_5^{0\mu\nu\rho\sigma\gamma} \\ K_5^{-\mu\nu\rho\sigma\gamma} & \bar{K}_5^{0\mu\nu\rho\sigma\gamma} & \omega_{5N}^{\mu\nu\rho\sigma\gamma} \end{pmatrix},$$

$$B_1^\mu = \frac{1}{\sqrt{2}} \begin{pmatrix} \frac{h_1^\mu + b_1^{0\mu}}{\sqrt{2}} & b_1^{+\mu} & K_{1,B}^{+\mu} \\ b_1^{-\mu} & \frac{h_1^\mu - b_1^{0\mu}}{\sqrt{2}} & K_{1,B}^{0\mu} \\ K_{1,B}^{-\mu} & \bar{K}_{1,B}^{0\mu} & h_1^\mu \end{pmatrix}.$$

TABLE IV: The partial decay channels of the ω_J/ρ_J ($J = 2, 4, 5$) mesons [15].

$\omega_2(1975)$		$\rho_2(1940)$		$\omega_4(2250)$		$\rho_4(2230)$		$\omega_5(2250)$		$\rho_5(2350)$	
Channel	BR	Channel	BR	Channel	BR	Channel	BR	Channel	BR	Channel	BR
$\pi\rho(1450)$	0.48	$\pi a_2(1320)$	0.25	$a_1\rho$	0.35	ρb_1	0.27	ρa_2	0.58	ρf_2	0.24
$\pi\rho$	0.24	$\pi\omega(1420)$	0.21	$a_2\rho$	0.30	$\rho\rho$	0.20	ωf_2	0.23	ωa_2	0.24
πb_1	0.11	$\pi\omega$	0.15	ωf_2	0.13	ρf_2	0.10	πb_1	0.09	ρb_1	0.13
$\pi\rho_3(1690)$	0.07	$\pi h_1(1170)$	0.10	$\pi\rho$	0.06	πa_1	0.09	πa_1	0.04	$\rho\rho$	0.09
$\omega\eta$	0.03	$\rho\eta$	0.07	$\pi\rho(1700)$	0.05	ωa_1	0.09	$\rho\pi$	0.03	$\pi\pi_2$	0.07
$\pi\rho(1700)$	0.02	$\pi a_0(1450)$	0.06	ωf_1	0.04	ωa_2	0.06	ηh_1	0.01	πa_2	0.07
KK^*	0.02	$\rho\rho$	0.05	$\rho\rho$	0.03	πa_2	0.04			πh_1	0.05
$KK^*(1410)$	0.02	KK^*	0.04			$\pi\omega$	0.01			πa_1	0.04
		$KK_2^*(1430)$	0.03							$\pi\omega$	0.01
		$\rho\eta'$	0.03								

The Lagrangian for $\omega_5 b_1 \pi$ vertex can be expressed in the following specific form:

$$\mathcal{L}_{\omega_5 b_1 \pi} = \frac{1}{2} g_{\omega_5 b_1 \pi} \omega_5^{\sigma\alpha\beta\gamma\delta} b_{1,\sigma}^+ \partial_\alpha \partial_\beta \partial_\gamma \partial_\delta \pi^- . \quad (23)$$

The $b_1 NN$ vertex is adopted from Ref. [36]:

$$\mathcal{L}_{b_1 NN} = \frac{i f_{b_1 NN}}{m_{b_1}} [\bar{N} \sigma_{\mu\nu} \gamma_5 N] \partial^\nu b_1^\mu . \quad (24)$$

$\pi^- p \rightarrow \rho_5(2350)p$ [Fig. 7(f)]. Here the exchange of an h_1 meson is involved, following the QPC prediction that πh_1 is the most important π -containing channel. The effective Lagrangian is

$$\mathcal{L}_{W_5 B_1 P} = g_{W_5 B_1 P} \text{tr} [W_5^{\mu\alpha\beta\gamma\delta} \{B_{1,\mu}, \partial_\alpha \partial_\beta \partial_\gamma \partial_\delta P\}_+]. \quad (25)$$

The Lagrangian for $\rho_5 h_1 \pi$ vertex can be expressed in the following specific form:

$$\mathcal{L}_{\rho_5 h_1 \pi} = \frac{1}{2} g_{\rho_5 h_1 \pi} \rho_5^{\mu\alpha\beta\gamma\delta} h_{1,\mu} \partial_\alpha \partial_\beta \partial_\gamma \partial_\delta \pi^- . \quad (26)$$

The $h_1 NN$ vertex, which has the same tensor structure as Eq. (24), is also taken from Ref. [36].

All coupling constants for the vertices appearing in the above Lagrangians are listed in Table V.

Using the effective Lagrangians introduced in the previous section, we write the tree-level amplitudes for the six reactions as follows.

$\pi^- p \rightarrow \omega_2(1975)n$ via t -channel ρ exchange:

$$i\mathcal{M}_{\omega_2} = -\frac{i}{2} g_{\omega_2 \rho \pi} \varepsilon^{\alpha\beta\gamma\delta} (k_2) (k_{1\beta}) \frac{-i(g_\alpha^\mu + q_\mu q_\alpha / m_\rho^2)}{t - m_\rho^2} \times \bar{u}(p_2) \left(g_{\rho NN} \gamma_\mu + \frac{f_{\rho NN}}{2m_p} \gamma_\mu \not{q} \right) u(p_1) F_t(q), \quad (27)$$

TABLE V: Coupling constants used in this work. The values in the left column are the three-meson couplings determined in this work by fitting the decay widths from Table IV. Those in the right column are the meson-nucleon-nucleon couplings taken from Ref. [36]. They correspond to the upper and lower vertices, respectively, in the Feynman diagrams of Fig. 7.

$g_{\rho_2 \omega \pi} = 5.89$	$g_{\omega NN} = 11.04$
	$f_{\omega NN} = -2.02$
$g_{\omega_2 \rho \pi} = 4.39$	$g_{\rho NN} = 2.05$
$g_{\omega_4 \rho \pi} = 3.91 \text{ GeV}^{-2}$	$f_{\rho NN} = 13.40$
$g_{\rho_4 a_1 \pi} = 18.82 \text{ GeV}^{-4}$	$g_{a_1 NN} = -2.90$
	$f_{a_1 NN} = -5.86$
$g_{\omega_5 b_1 \pi} = 45.16 \text{ GeV}^{-3}$	$f_{b_1 NN} = -8.01$
$g_{\rho_5 h_1 \pi} = 55.27 \text{ GeV}^{-3}$	$f_{h_1 NN} = -0.29$

$\pi^- p \rightarrow \rho_2(1940)p$ via t -channel ω exchange:

$$i\mathcal{M}_{\rho_2} = -\frac{i}{2} g_{\rho_2 \omega \pi} \varepsilon^{\alpha\beta\gamma\delta} (k_2) (k_{1\beta}) \frac{-i(g_\alpha^\mu + q_\mu q_\alpha / m_\omega^2)}{t - m_\omega^2} \times \bar{u}(p_2) \left(g_{\omega NN} \gamma_\mu + \frac{f_{\omega NN}}{2m_p} \gamma_\mu \not{q} \right) u(p_1) F_t(q), \quad (28)$$

$\pi^- p \rightarrow \omega_4(2250)n$ via t -channel ρ exchange:

$$i\mathcal{M}_{\omega_4} = \frac{i}{2} g_{\omega_4 \rho \pi} k_{1\alpha} k_{1\beta} k_{1\gamma} \varepsilon^{\sigma\alpha\beta\gamma\delta} (k_2) \frac{-i(g_\sigma^\mu + q^\mu q_\sigma / m_\rho^2)}{t - m_\rho^2} \times \bar{u}(p_2) \left[g_{\rho NN} \gamma_\mu + \frac{f_{\rho NN}}{2m_p} \gamma_\mu \not{q} \right] u(p_1) F_t(q), \quad (29)$$

$\pi^- p \rightarrow \rho_4(2230)n$ via t -channel a_1 exchange:

$$i\mathcal{M}_{\rho_4} = -\frac{1}{2} g_{\rho_4 a_1 \pi} \epsilon_{\mu\nu\rho\sigma} q^\nu k_{1\alpha} k_{1\beta} k_{1\gamma} k_1^\sigma \epsilon^{\mu\alpha\beta\gamma*}(k_2) \frac{-i(g_\rho^\xi + q^\xi q_\rho/m_{a_1}^2)}{t - m_{a_1}^2} F_t(q) \times \bar{u}(p_2) \left(g_{a_1 NN} \gamma_\xi \gamma_5 - \frac{f_{a_1 NN}}{M_p} \gamma_5 \not{q} \right) u(p_1), \quad (30)$$

$\pi^- p \rightarrow \omega_5(2250)n$ via t -channel b_1 exchange:

$$i\mathcal{M}_{\omega_5} = \frac{1}{2} \frac{f_{b_1 NN}}{m_{b_1}} g_{\omega_5 b_1 \pi} k_{1\alpha} k_{1\beta} k_{1\gamma} k_{1\delta} \epsilon^{\sigma\alpha\beta\gamma\delta*}(k_2) \times \frac{-i(g_\sigma^\mu + q^\mu q_\sigma/m_{b_1}^2)}{t - m_{b_1}^2} \bar{u}(p_2) \sigma_{\mu\nu} \gamma_5 u(p_1) \times q^\nu F_t(q), \quad (31)$$

$\pi^- p \rightarrow \rho_5(2350)n$ via t -channel h_1 exchange:

$$i\mathcal{M}_{\rho_5} = -\frac{1}{2} \frac{f_{h_1 NN}}{m_{h_1}} g_{\rho_5 h_1 \pi} k_{1\alpha} k_{1\beta} k_{1\gamma} k_{1\delta} \epsilon^{\sigma\alpha\beta\gamma\delta*}(k_2) \times \frac{-i(g_\sigma^\mu + q^\mu q_\sigma/m_{h_1}^2)}{t - m_{h_1}^2} \bar{u}(p_2) \sigma_{\mu\nu} \gamma_5 u(p_1) \times q^\nu F_t(q). \quad (32)$$

In the above expressions, $\epsilon(k_2)$ denotes the polarization tensor of the outgoing high-spin meson. $\bar{u}(p_2)$ and $u(p_1)$ are the Dirac spinors of the outgoing and incoming nucleons, respectively. $t = q^2 = (k_1 - k_2)^2$ is the squared four-momentum transfer. The form factor $F_t(q)$ is taken from Eq. (9) with the same cutoff $\Lambda_t = 3.5 \pm 0.5$ GeV used for the $J = 3$ states.

The t -channel propagators are Reggeized according to Eq. (10). The corresponding Regge trajectories for the exchanged mesons are

$$\alpha_R(t) = 1 + \alpha'_R (t - m_R^2), \quad R = \rho, \omega, a_1, b_1, h_1, \quad (33)$$

with slopes $\alpha'_\rho = 0.8$ GeV⁻² [29], $\alpha'_\omega = 0.9$ GeV⁻² [29], $\alpha'_{a_1} = 0.8$ GeV⁻² (determined from the mass of the $a_3(1875)$ state following Ref. [37]), $\alpha'_{b_1} = 0.7$ GeV⁻² [30], and $\alpha'_{h_1} = 0.7$ GeV⁻² [30].

With the amplitudes (Eqs. (29)–(32)) and the differential cross-section formula in Eq. (14), we can now compute the total and differential cross sections for the six states.

Total cross sections. The total cross sections for meson–nucleon production of the $J = 2$ states $\omega_2(1975)$ and $\rho_2(1940)$, the $J = 4$ states $\omega_4(2250)$ and $\rho_4(2230)$, and the $J = 5$ states $\omega_5(2250)$ and $\rho_5(2350)$ via t -channel exchange are shown in Fig. 8 as functions of the center-of-mass energy \sqrt{s} . The solid curves correspond to a central cutoff $\Lambda_t = 3.5$ GeV, with the shaded bands representing the uncertainty from varying Λ_t by ± 0.5 GeV.

For the $J = 2$ states, subplots (a) and (d) illustrate clear spin-isospin patterns. The $\omega_2(1975)$ cross section peaks at approximately $0.7 \mu\text{b}$ near $\sqrt{s} \approx 3.6$ GeV, while the $\rho_2(1940)$

cross section exhibits a significantly larger peak of about $6.5 \mu\text{b}$ at a similar energy. This order-of-magnitude difference in peak cross sections for states with identical spin $J = 2$ but different isospin underscores a strong isospin dependence in the production mechanisms. Both curves show a broad peak structure followed by a monotonic decline at high \sqrt{s} . A clear spin-dependent and isospin-dependent pattern is observed. The $J = 4$ cross sections [subplots (b) and (e)] are of the order of 0.1 – $0.3 \mu\text{b}$. $\omega_4(2250)$ exhibits a broad peak of about $0.25 \mu\text{b}$ near $\sqrt{s} = 4.3$ GeV, while $\rho_4(2230)$ peaks at a lower value of approximately $0.14 \mu\text{b}$. In contrast, the $J = 5$ cross sections [subplots (c) and (f)] display a significant isospin splitting. The $\omega_5(2250)$ cross section reaches a maximum of about $0.68 \mu\text{b}$, comparable to the $J = 4$ cross sections, whereas $\rho_5(2350)$ is strongly suppressed, with a peak of only about $0.0025 \mu\text{b}$. The suppression of the ρ_5 state, despite its higher mass, is a notable feature that may be attributed to the specific coupling structure and the higher derivative nature of the interaction vertices for this channel. All curves decline monotonically at high \sqrt{s} , consistent with t -channel exchange kinematics. The narrow uncertainty bands indicate that the predictions are robust under variations of the cutoff parameter.

Differential cross sections. The angular distributions are presented in Fig. 9, which shows $d\sigma/d\cos\theta$ for the six states at center-of-mass energies $W = 3.5, 4.0, 5.0,$ and 6.0 GeV.

All panels in Fig. 9 share two key features of t -channel processes: (i) a very strong forward peak ($\cos\theta \rightarrow 1$) at all energies, and (ii) the forward peak narrows with increasing energy. This reflects the kinematics of meson exchange, where small momentum transfer favors scattering at very small angles.

A closer inspection reveals significant effects of both spin and isospin. For the $J = 2$ resonances, a clear isospin splitting is observed. The $\omega_2(1975)$ [Fig. 9(a)] exhibits forward differential cross sections on the order of $10 \mu\text{b}$ across the measured energy range. In contrast, its isospin partner, the $\rho_2(1940)$ [Fig. 9(d)], displays a consistently larger magnitude, with forward cross sections on the order of $10^2 \mu\text{b}$. This indicates that the production of the isovector ρ_2 state is significantly enhanced compared to the isoscalar ω_2 state for $J = 2$.

The $J = 4$ state $\omega_4(2250)$ [Fig. 9(b)] reaches differential cross sections of up to about $10 \mu\text{b}$ in the extreme forward direction, while its isospin partner $\rho_4(2230)$ [Fig. 9(e)] shows a similar shape but with a slightly gentler slope and a lower peak magnitude. The $J = 5$ states [Figs. 9(c) and (f)] exhibit the expected strong suppression, particularly for the $\rho_5(2350)$ state.

IV. SUMMARY

In this work, we have performed a systematic study of the production of high-spin ω_J and ρ_J mesons ($J = 2, 3, 4, 5$) in $\pi^- p$ scattering, employing an effective Lagrangian approach. Our primary goal was to provide theoretical predictions for the production dynamics of these states, which are far less explored than their decay properties.

Our analysis is based on a unified framework that con-

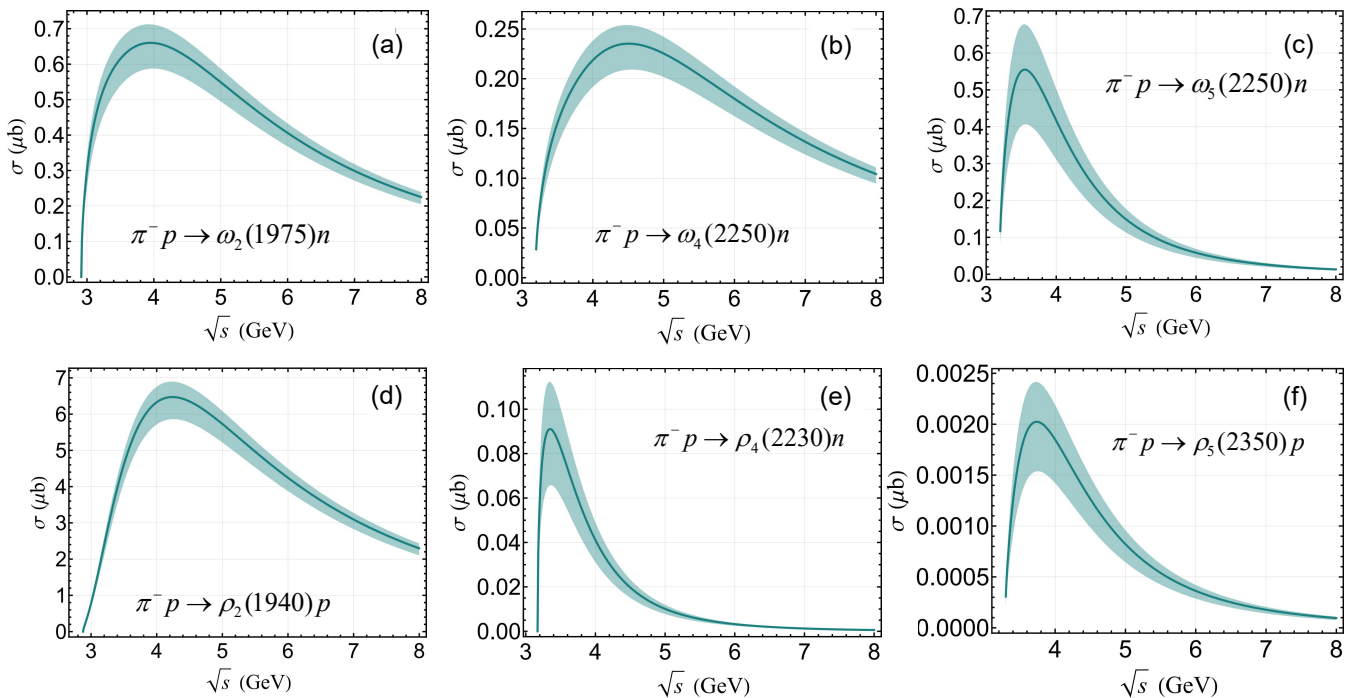


FIG. 8: The energy dependence of the total cross section for production of the $\omega_2(1975)$, $\rho_2(1940)$, $\omega_4(2250)$, $\rho_4(2230)$, $\omega_5(2250)$, $\rho_5(2350)$ through t -channel with cutoff $\Lambda_t = 3.5 \pm 0.5$ GeV.

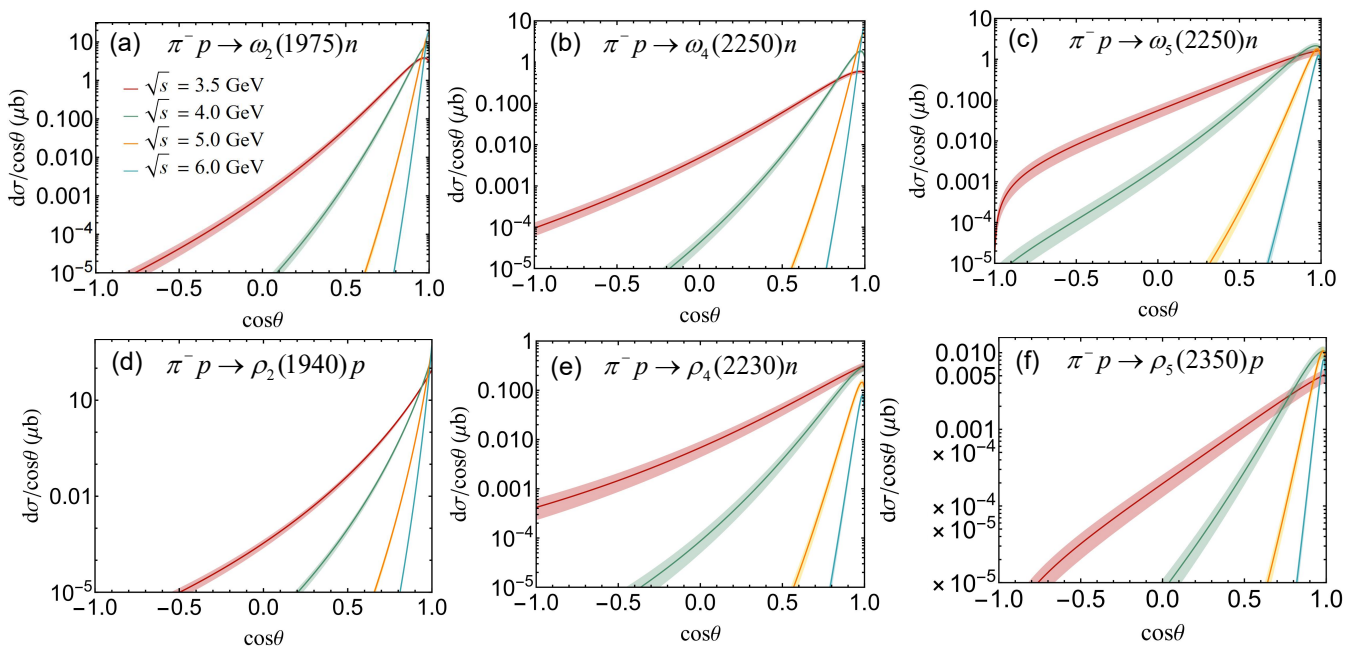


FIG. 9: The differential cross section $d\sigma/d\cos\theta$ of the $\omega_2(1975)$, $\rho_2(1940)$, $\omega_4(2250)$, $\rho_4(2230)$, $\omega_5(2250)$, $\rho_5(2350)$ production at different c.m. energies $W = 3.5, 4, 5$ and 6 GeV.

considers only the dominant t -channel meson-exchange mechanisms. For each channel, the exchanged meson (e.g., ρ , π , ω , a_1 , b_1 , or h_1) is selected according to the π -containing decay modes predicted by the QPC model. For the well-established $J = 3$ states $\omega_3(1670)$ and $\rho_3(1690)$, the model

has a single adjustable parameter: the form-factor cutoff Λ_t . A fit to the available total and differential cross-section data yields $\Lambda_t = 3.5 \pm 0.5$ GeV. Using this determined parameter, we subsequently made parameter-free predictions for the production of their lower-spin and higher-spin partners $\omega_2(1975)$,

$\rho_2(1940)$, $\omega_4(2250)$, $\rho_4(2230)$, $\omega_5(2250)$, and $\rho_5(2350)$. The high-energy behavior is consistently described by applying Reggeization to the t -channel propagators.

The key findings of this study are as follows:

1. The model with $\Lambda_t = 3.5 \pm 0.5$ GeV provides an excellent description of the existing total and differential cross-section data for $\pi^- p \rightarrow \omega_3(1670)n$ and $\pi^- p \rightarrow \rho_3(1690)n$, validating the theoretical framework.
2. The predicted cross sections for the higher-spin ($J = 4, 5$) states are systematically suppressed compared to the $J = 3$ case, an expected consequence of the higher derivative couplings in the production vertices. Crucially, all predicted cross sections remain in the experimentally accessible range.
3. The differential cross sections for all states exhibit a pronounced forward peak ($\cos \theta \rightarrow 1$), a distinctive signature of the t -channel production mechanism.
4. The consistent description of eight different resonance production channels with a single universal parameter demonstrates the robustness of the model. It provides a coherent picture linking the decay properties (from the QPC model) to the production dynamics in scattering experiments.

In conclusion, this work provides the first comprehensive set of theoretical predictions for the production cross sections of the high-spin ω_2 , ρ_2 , ω_4 , ρ_4 , ω_5 , and ρ_5 states in $\pi^- p$ reactions. The results offer concrete, testable guidance for future

experimental searches at facilities such as J-PARC and COMPASS, particularly in the forward-angle region where the cross sections are largest. This analysis bridges spectroscopy and production studies, supporting future meson-beam experiments in completing the spectrum of light hadrons.

Acknowledgments

T.Y.L. would like to thank Yu Zhuge, Shahriyar Jafarzade, and Xiao-Yun Wang for their useful discussions. This work is also supported by the National Natural Science Foundation of China under Grant Nos. 12335001 and 12247101, the ‘111 Center’ under Grant No. B20063, the Natural Science Foundation of Gansu Province (No. 22JR5RA389, No. 25JRRA799), the fundamental Research Funds for the Central Universities, the project for top-notch innovative talents of Gansu province, and Lanzhou City High-Level Talent Funding.

APPENDIX: EXPLICIT EXPRESSIONS OF PROPAGATORS

The propagator of a field for a boson field can be written as

$$S(p) = \frac{1}{p^2 - M^2} (\not{p} + M) \Delta_{\alpha_1 \dots \alpha_{n-1}}^{\beta_1 \dots \beta_{n-1}}(j, p). \quad (34)$$

The explicit expressions for the projection operators of fields from spin-3 to spin-5 are given as follows [38, 39].

$$\Delta_{\alpha_1 \alpha_2}^{\beta_1 \beta_2}(2, p) = \frac{1}{2} \left(\bar{g}_{\alpha_1}^{\beta_1} \bar{g}_{\alpha_2}^{\beta_2} + \bar{g}_{\alpha_1}^{\beta_2} \bar{g}_{\alpha_2}^{\beta_1} - \frac{2}{3} \bar{g}_{\alpha_1 \alpha_2} \bar{g}^{\beta_1 \beta_2} \right). \quad (35)$$

$$\begin{aligned} \Delta_{\alpha_1 \alpha_2 \alpha_3}^{\beta_1 \beta_2 \beta_3}(3, p) &= -\frac{1}{36} \sum_{P(\alpha), P(\beta)} \left(\bar{g}_{\alpha_1}^{\beta_1} \bar{g}_{\alpha_2}^{\beta_2} \bar{g}_{\alpha_3}^{\beta_3} - \frac{3}{5} \bar{g}_{\alpha_1 \alpha_2} \bar{g}^{\beta_1 \beta_2} \bar{g}_{\alpha_3}^{\beta_3} \right) \\ &= -\frac{1}{6} \left(\bar{g}_{\alpha_1}^{\beta_1} \bar{g}_{\alpha_2}^{\beta_2} \bar{g}_{\alpha_3}^{\beta_3} + \bar{g}_{\alpha_1}^{\beta_1} \bar{g}_{\alpha_2}^{\beta_3} \bar{g}_{\alpha_3}^{\beta_2} + \bar{g}_{\alpha_1}^{\beta_2} \bar{g}_{\alpha_2}^{\beta_1} \bar{g}_{\alpha_3}^{\beta_3} + \bar{g}_{\alpha_1}^{\beta_2} \bar{g}_{\alpha_2}^{\beta_3} \bar{g}_{\alpha_3}^{\beta_1} + \bar{g}_{\alpha_1}^{\beta_3} \bar{g}_{\alpha_2}^{\beta_1} \bar{g}_{\alpha_3}^{\beta_2} + \bar{g}_{\alpha_1}^{\beta_3} \bar{g}_{\alpha_2}^{\beta_2} \bar{g}_{\alpha_3}^{\beta_1} \right) \\ &\quad + \frac{1}{15} \left[\bar{g}_{\alpha_1 \alpha_2} \left(\bar{g}^{\beta_1 \beta_2} \bar{g}_{\alpha_3}^{\beta_3} + \bar{g}^{\beta_1 \beta_3} \bar{g}_{\alpha_3}^{\beta_2} + \bar{g}^{\beta_2 \beta_3} \bar{g}_{\alpha_3}^{\beta_1} \right) + \bar{g}_{\alpha_1 \alpha_3} \left(\bar{g}^{\beta_1 \beta_2} \bar{g}_{\alpha_2}^{\beta_3} + \bar{g}^{\beta_1 \beta_3} \bar{g}_{\alpha_2}^{\beta_2} + \bar{g}^{\beta_2 \beta_3} \bar{g}_{\alpha_2}^{\beta_1} \right) \right. \\ &\quad \left. + \bar{g}_{\alpha_2 \alpha_3} \left(\bar{g}^{\beta_1 \beta_2} \bar{g}_{\alpha_1}^{\beta_3} + \bar{g}^{\beta_1 \beta_3} \bar{g}_{\alpha_1}^{\beta_2} + \bar{g}^{\beta_2 \beta_3} \bar{g}_{\alpha_1}^{\beta_1} \right) \right], \end{aligned} \quad (36)$$

$$\Delta_{\alpha_1 \alpha_2 \alpha_3 \alpha_4}^{\beta_1 \beta_2 \beta_3 \beta_4}(4, p) = \frac{1}{576} \sum_{P(\alpha), P(\beta)} \left(\bar{g}_{\alpha_1}^{\beta_1} \bar{g}_{\alpha_2}^{\beta_2} \bar{g}_{\alpha_3}^{\beta_3} \bar{g}_{\alpha_4}^{\beta_4} - \frac{6}{7} \bar{g}_{\alpha_1 \alpha_2} \bar{g}^{\beta_1 \beta_2} \bar{g}_{\alpha_3}^{\beta_3} \bar{g}_{\alpha_4}^{\beta_4} + \frac{3}{35} \bar{g}_{\alpha_1 \alpha_2} \bar{g}_{\alpha_3 \alpha_4} \bar{g}^{\beta_1 \beta_2} \bar{g}^{\beta_3 \beta_4} \right), \quad (37)$$

$$\begin{aligned} \Delta_{\alpha_1 \alpha_2 \alpha_3 \alpha_4 \alpha_5}^{\beta_1 \beta_2 \beta_3 \beta_4 \beta_5}(5, p) &= -\left(\frac{1}{120} \right)^2 \sum_{P(\alpha), P(\beta)} \left(\bar{g}_{\alpha_1}^{\beta_1} \bar{g}_{\alpha_2}^{\beta_2} \bar{g}_{\alpha_3}^{\beta_3} \bar{g}_{\alpha_4}^{\beta_4} \bar{g}_{\alpha_5}^{\beta_5} - \frac{10}{9} \bar{g}_{\alpha_1 \alpha_2} \bar{g}^{\beta_1 \beta_2} \bar{g}_{\alpha_3}^{\beta_3} \bar{g}_{\alpha_4}^{\beta_4} \bar{g}_{\alpha_5}^{\beta_5} + \frac{5}{21} \bar{g}_{\alpha_1 \alpha_2} \bar{g}_{\alpha_3 \alpha_4} \bar{g}^{\beta_1 \beta_2} \bar{g}^{\beta_3 \beta_4} \bar{g}_{\alpha_5}^{\beta_5} \right), \end{aligned} \quad (38)$$

where $\bar{g}_{\mu\nu}$ as

$$\bar{g}_{\mu\nu} = g_{\mu\nu} - \frac{1}{p^2} p_\mu p_\nu. \quad (39)$$

- [1] S. Navas et al. (Particle Data Group), *Phys. Rev. D* **110**, 030001 (2024).
- [2] X. WANG and X. LIU, *Nucl. Phys. Rev.* **42**, 10 (2025).
- [3] Y. Hou, Y. Gao, and X.-Y. Wang, *Nucl. Phys. A* **1050**, 122925 (2024).
- [4] X.-Y. Wang, H.-F. Zhou, and X. Liu, *Phys. Rev. D* **110**, 014026 (2024), arXiv:2404.11078 [hep-ph] .
- [5] X.-Y. Wang, H.-F. Zhou, and X. Liu, *Phys. Rev. D* **108**, 034015 (2023), arXiv:2306.12815 [hep-ph] .
- [6] X.-Y. Wang, F.-C. Zeng, and X. Liu, *Phys. Rev. D* **106**, 036005 (2022), arXiv:2205.09283 [hep-ph] .
- [7] X.-Y. Wang and J. He, *Eur. Phys. J. A* **55**, 152 (2019), arXiv:1909.07631 [nucl-th] .
- [8] X.-Y. Wang, J. He, Q. Wang, and H. Xu, *Phys. Rev. D* **99**, 014020 (2019), arXiv:1810.04096 [hep-ph] .
- [9] Q.-Y. Guo, J. Liu, P. Wu, and D.-Y. Chen, *Phys. Rev. C* **112**, 065201 (2025).
- [10] A. V. Anisovich, V. V. Anisovich, and A. V. Sarantsev, *Phys. Rev. D* **62**, 051502 (2000), arXiv:hep-ph/0003113 .
- [11] L.-P. He, X. Wang, and X. Liu, *Phys. Rev. D* **88**, 034008 (2013), arXiv:1306.5562 [hep-ph] .
- [12] Z.-Y. Bai, Q.-S. Zhou, and X. Liu, *Phys. Rev. D* **111**, 054013 (2025), arXiv:2502.05754 [hep-ph] .
- [13] T.-y. Li, Y.-r. Wang, and C.-q. Pang, *Phys. Rev. D* **107**, 074008 (2023), arXiv:2205.02157 [hep-ph] .
- [14] Y.-R. Wang, T.-Y. Li, Z.-Y. Fang, H. Chen, and C.-Q. Pang, *Phys. Rev. D* **106**, 114024 (2022), arXiv:2208.10329 [hep-ph] .
- [15] C.-Q. Pang, B. Wang, X. Liu, and T. Matsuki, *Phys. Rev. D* **92**, 014012 (2015), arXiv:1505.04105 [hep-ph] .
- [16] N. Armenise, A. Forino, and A. M. Cartacci, *Phys. Lett. B* **26**, 336 (1968).
- [17] M. J. Corden et al., *Nucl. Phys. B* **138**, 235 (1978).
- [18] A. Engler, R. W. Kraemer, S. Toaff, F. Weisser, J. Diaz, F. A. DiBianca, W. J. Fickinger, and D. K. Robinson, *Phys. Rev. D* **10**, 2070 (1974).
- [19] S. Jafarzade, A. Koenigstein, and F. Giacosa, *Phys. Rev. D* **103**, 096027 (2021), arXiv:2101.03195 [hep-ph] .
- [20] M. M. Nagels, T. A. Rijken, and Y. Yamamoto, *Phys. Rev. C* **99**, 044003 (2019), arXiv:1501.06636 [nucl-th] .
- [21] J. Diaz et al., *Phys. Rev. Lett.* **32**, 260 (1974).
- [22] J. A. J. Matthews, J. D. Prentice, T. S. Yoon, J. T. Carroll, M. W. Firebaugh, and W. D. Walker, *Phys. Rev. D* **3**, 2561 (1971).
- [23] I. R. Kenyon, J. B. Kinson, J. M. Scarr, I. O. Skillicorn, H. O. Cohn, R. D. McCulloch, W. M. Bugg, G. T. Condo, and M. M. Nussbaum, *Phys. Rev. Lett.* **23**, 146 (1969).
- [24] G. Costa et al. (BARI-BONN-CERN-GLASGOW-LIVERPOOL-MILAN-VIENNA), *Nucl. Phys. B* **175**, 402 (1980).
- [25] W. Blum et al. (CERN-MUNICH), *Phys. Lett. B* **57**, 403 (1975).
- [26] D. Alde et al. (GAMS), *Nuovo Cim. A* **107**, 1867 (1994).
- [27] S. Ozaki, H. Nagahiro, and A. Hosaka, *Phys. Rev. C* **81**, 035206 (2010), arXiv:0910.0384 [hep-ph] .
- [28] J. K. Storrow, *Phys. Rept.* **103**, 317 (1984).
- [29] M. Guidal, J. M. Laget, and M. Vanderhaeghen, *Nucl. Phys. A* **627**, 645 (1997).
- [30] A.-C. Wang, N.-C. Wei, and F. Huang, *Phys. Rev. C* **111**, 025205 (2025), arXiv:2502.11499 [hep-ph] .
- [31] A. V. Anisovich, C. A. Baker, C. J. Batty, D. V. Bugg, L. Montanet, V. A. Nikonov, A. V. Sarantsev, V. V. Sarantsev, and B. S. Zou, *Phys. Lett. B* **542**, 19 (2002), arXiv:1109.5817 [hep-ex] .
- [32] A. V. Anisovich, C. A. Baker, C. J. Batty, D. V. Bugg, L. Montanet, V. A. Nikonov, A. V. Sarantsev, V. V. Sarantsev, and B. S. Zou, *Phys. Lett. B* **542**, 8 (2002), arXiv:1109.5247 [hep-ex] .
- [33] A. V. Anisovich, C. A. Baker, C. J. Batty, D. V. Bugg, V. A. Nikonov, A. V. Sarantsev, V. V. Sarantsev, and B. S. Zou, *Phys. Lett. B* **507**, 23 (2001).
- [34] A. Hasan and D. V. Bugg, *Phys. Lett. B* **334**, 215 (1994).
- [35] A. A. Carter, *Nucl. Phys. B* **141**, 467 (1978).
- [36] T. A. Rijken, M. M. Nagels, and Y. Yamamoto, *Prog. Theor. Phys. Suppl.* **185**, 14 (2010).
- [37] G. Galata, *Phys. Rev. C* **83**, 065203 (2011), arXiv:1102.2070 [hep-ph] .
- [38] M. Döring, J. Haidenbauer, M. Mai, and T. Sato, *Prog. Part. Nucl. Phys.* **146**, 104213 (2026), arXiv:2505.02745 [nucl-th] .
- [39] S.-H. Kim, Y. Oh, S. Son, S. Sakinah, and M.-K. Cheoun, *Phys. Rev. D* **111**, 054031 (2025), arXiv:2412.18927 [hep-ph] .